Deep Resistivity Tomographic Imaging of

The Qualibou Caldera, Saint Lucia

Frank Dale Morgan[1], Yervant Vichabian[1], and John Sogade[1]

---

[1] Earth Resources Laboratory, Department of Earth, Atmospheric, and Planetary Sciences, Massachusetts Institute of Technology, 42 Carleton Street, E34-462, Cambridge MA 02142.

Abstract

The Qualibou Caldera has been studied since the 1970's for possible development of geothermal power generation. In 1974 dipole-dipole resistivity measurements were performed in the area. The apparent resistivity data was plotted as contours and a single line running through Sulphur Springs was interpreted by using forward models to generate a best fit model. The data is reanalyzed using a robust 2D inversion method. The result shows a resistive body beneath Sulphur Springs, the presence of which has been debated for nearly thirty years. The data from all 2D tomograms is interpolated into 3D, which generates images showing conductive features reminiscent of hydrothermal convection plumes.

Qualibou Caldera (Sulphur Springs)

Introduction

Saint Lucia is part of the Lesser Antilles volcanic island arc located in the eastern Caribbean (Figure 1). Volcanic activity has been concentrated in the southern half of the island for the last several million years (Wohletz, et. al., 1986). The Sulphur Springs geothermal area lies within what has been identified as the Qualibou Caldera, which is a large topographic depression, formed by downfaulting and the caldera structure. There is an abundance of natural manifestations, several hot springs, and microseismic activity in the area as evidence of a geothermal system. The Government of Saint Lucia has been interested in developing the area for production and several geothermal investigations have been conducted starting from 1960s to the present (Greenwood and Lee, 1976; Merz and McLellan, 1977; Aquater, 1982; LANL, 1984; GENZL, 1992). However, the area has not yet seen any development towards geothermal production. The investigations have confirmed a high temperature geothermal system under Sulphur Springs but with highly corrosive chemistry, which makes development there unfeasible.

The Earth Resources Laboratory (ERL) at the Massachusetts Institute of Technology (MIT) has been studying the geothermal resources of Sulphur Springs for several years including several expeditions to the Saint Lucia. Upon finding the work of Greenwood and Lee (1976), it was decided to reinterpret the resistivity data to generate modern 2D tomographic images. The motivation for the work was to determine if a resistive body

existed beneath Sulphur Springs and to possibly image circulation fluids in the geothermal system.

Geology

The known volcanic history of southern Saint Lucia spans over 8 Ma and is made up of several periods of eruptive activity. In the area of the Qualibou Caldera there are: (1) 5 to 6 Ma old basaltic lava flows, overlain by andesitic to dacitic composite cones 0.75 to 1 Ma old; (2) caldera related rocks that consist of andesitic to dacitic tephra falls and pyroclastic flows ~ 0.04 Ma; (3) intracaldera dacitic tephra and lava domes ~ 0.02 to 0.032 Ma. The most recent activity in 1766 was at the Sulphur Springs consisting of steam explosions. Figure 2 shows the geology of the area from Greenwood and Lee (1976).

Structure

A complex structural pattern exists (Figure 3) from the intersection of deep, linear, regional, vertical faults with curvilinear, moderate to low angle local faults associated with caldera collapse (Aquater, 1982). Two major regional faults trending ENE occur adjacent to the Qualibou Caldera effectively bounding the caldera. The northernmost one parallels Ravine Toraille and cuts the north slopes of Mt. Gimie, and the southernmost is parallel to the drainage of the L'Ivrogne River. There are also parallel to small graben forming faults such as those in Fond St. Jacque and Fond Cannes. Overall movement on

the faults is dominantly vertical with little variation in trend. Present day drainage follows these faults lines, often cutting into significant thicknesses of tuff. The deep projection of regional faults is best evidenced by the alignment of vents along them, such as the NE-SW alignments of two major edifices: Mt. Gimie, Terre Blanche, Petit Piton and Gros Piton, Fond Doux, Belfond. Less developed NW-SE faults occur along the Migny River and near Anse Chastanet. This latter fault extends across Soufriere Bay and well into the Sulphur Springs area and may project across the caldera.

Hydrogeochemistry

There are three thermal springs (Diamond, Cresslands, and Malgretoute) north and west of the Sulphur Springs, which have been analyzed by Bath (1976), Aquater (1982), LANL (1984), Goff and Vuataz (1984). The striking fact about the chemistry of these springs is their general resemblance to steam condensate water at Sulphur Springs (LANL, 1984). They contain high HCO_3^-, high B, variable SO_4^{--}, and relatively low Cl. Analyzed values of B, Cl, and F in Diamond Spring are identical to those of cauldron springs at Sulphur Springs, suggesting they have been formed by similar processes. Waters of this type form along the cooler margins and tops of deep geothermal systems by condensation of CO_2 rich steam (LANL, 1984).

Tritium (^3H) is an isotopic tracer produced during atmospheric nuclear testing from 1953 to 1964. Tritium is very useful in tracing groundwater flow because of its short half-life of 12.3 years (Goff and Vuataz, 1984). At Sulphur Springs drowned fumaroles have the lowest values at less than 1 as they are composed almost entirely of condensed steam

from a deep reservoir. The pools and flowing springs, which are mixed with surface waters, show tritium values of 3 to 5 similar to the surface waters. Presumably the deep geothermal reservoir contains water having 0 tritium (pre nuclear testing) with relatively older waters of at least greater than 30 years. The three thermal springs have low tritium values of 1 to 2 indicating they are composed mostly of older water with a residence time of greater than 20 years. These lower values indicate that they originate from a main condensation zone above the geothermal reservoir.

Leakage anomalies are comprised of volatile components CO_2, NH_3, and H_3BO_3, which are released with steam during boiling of geothermal fluids (Aquater, 1982). Sulphur Springs has very high values and three other areas contain measureable quantities (LANL, 1984): 1) the zone northwest and north of Sulphur Springs (Malgretoute to Diamond); 2) the north caldera collapse zone (Diamond Springs to Cresslands); 3) the southwest caldera collapse zone (Fond Doux to Gros Piton). The quantity of these components decreases from area 1 to 3, area 3 is very weakly anomalous. The data suggests major upflow of fluids at Sulphur Springs and lateral flow to the north and northwest.

Summary of Geothermal Convection Systems

In convection systems most heat is transferred by circulation fluids rather than by conduction. Convection is driven by a heat source at the base of the system. Heated fluid of low density tends to rise and be replaced by cooler fluid of higher density, which

is supplied from the margins of the system (Kruger and Otte, 1973). The two major types of convection systems are characterized by the dominant pressure controlling phase of the fluid; hot-water or dry-steam (vapor dominated).

Hot-water systems are characterized by liquid water as the pressure controlling fluid phase. Water serves as the medium by which heat is transferred from depth to shallower geothermal reservoirs (White, et al., 1971). Cool meteoric waters infiltrate the subsurface and are heated by conduction from hot rock driving fluids buoyantly upward. If the rocks have many interconnected pores or fractures of high permeability, the heated water rises rapidly to the surface and is dissipated. If the upward movement is impeded by rocks with few interconnected pores or fractures, geothermal energy may be stored in reservoirs below the impeding layer. Heat accounts for the density difference between cold, downward moving recharge water and hot, upwelling geothermal water.

Dry-steam or vapor-dominated systems produce dry or superheated steam with no associated liquid. These systems develop initially from hot-water systems characterized by very high heat supply and low rates of recharge (White, et al., 1971). When the heat supply of a developing system becomes great enough to boil off more water than is replenished a vapor-dominated reservoir begins to develop. The fraction of discharged fluids that exceeds the recharge is supplied by water previously stored in the larger fractures and pores**.** Only part of the steam is discharged at the surface as vapor; most of the total upflow recondenses to liquid on the margins of the reservoir creating convective circulation of fluids that feed back to the reservoir (Kruger and Otte, 1973).

Resistivity

Rock resistivity is mainly dependent on the pore fluid solution resistivity and on the quantity of fluid present. Geothermal regions typically generate circulating brines of low resistivity. Volcanic rocks such as Andesite, Dacite, are low in pore volume therefore they have high resistivities . Rocks in which the pore liquids have boiled, i.e. vapor dominated, are resistive because there is minimal liquid left. Significant resistivity contrasts exist between a geothermal source, associated fluids, and the surrounding material; hence resistivity is an excellent exploration tool.

Institute of Geological Sciences Investigation

Background

In the early 1970's, the Government of Saint Lucia requested assistance from the Overseas Development Ministry of England in developing an exploration program for geothermal resources in Sulphur Springs. A component of the program was a geophysical study conducted by Mr. Greenwood and Mr. Lee of the Institute of Geological Sciences (IGS). They performed 50 line Km of resistivity surveys in the area from September to December 1974.

Resistivity Equipment

The resistivity instrument used was a Scintrex 2.5 KW transmitter (type LPC-7) which generated a square wave with equal on and off times and remote triggered receiver (type RDC-8). An internal oscillator was synchronized with the transmitted current pulse triggering an acquisition gate on the receiver, thus locking the receiver and transmitter.

Dipole-Dipole Survey Lines

After experimenting with the Wenner Array and non-collinear dipole-dipole acquisition it was decided that the collinear dipole-dipole method was the only feasible approach considering the topography and extent of the survey. Thirteen individual lines were cut and pegged for a total of 50 line km of surveys shown in Figure 4. A map with the locations of relevant towns is shown in Figure 5. Employing a dipole spacing of 200 m the pseudo sections peered to a depth of 1 km.

Pseudo Sections

Figure 6 (from Greenwood and Lee, 1976) is a representative example of the resistivity data plotted as contour pseudo sections. Apparent resistivity values are low ranging from 3 to 500 ohm-m and typically less than 50 ohm-m. A general feature observed in the data is a decrease in apparent resistivity with an increase in depth, the only exception being Sulphur Springs. The area of the surface emanations has very low values of 3 to 5 ohm-m with a more resistive zone of 30 to 60 ohm-m at depths greater than 600 m. To the north and south of Sulphur Springs zones of apparent resistivity of 10 ohm-m and lower

extend laterally for several hundreds of meters at a depth approximately of sea level. The zone to the south appears to be "capped" by higher values of 50 to 500 ohm-m. The two zones are apparently separated by 30 ohm-m under Sulphur Springs.

Models – Interpretation

In 1975, the standard interpretation method for dipole-dipole data was to simply plot them as pseudo sections with no numerical processing. Inversion codes for true resistivities were not yet developed to be employed in the investigation. Two computer programs were used to make forward model interpretations. The first, RES1 (Lee, 1976), calculated theoretical apparent resistivity curves for horizontally layered structures of up to ten layers. The second, RESCAL (Geotronics Corporation), calculated apparent resistivity sections due to a two dimensional model made up of blocks of various resistivities. The resulting cross sections are compared with the field results, a new model is constructed, and so on until a satisfactory fit is achieved. Resistivity Line 9 was chosen for a detailed interpretation with these programs because it passes directly through Sulphur Springs. Figure 7 shows the best fit model of true resistivities for Line 9. This result was the best possible with the available technology in computer codes of that day.

Reinterpretation

Data Reconstruction

The actual data could not be obtained therefore the only available data was pseudo section contout plots of apparent resistivity from the Greenwood and Lee (1976) report. Each pseudo section plot had its "cross sections" of transmitter and receiver dipoles regenerated by hand drawing (Figure 8) and the corresponding apparent resistivity value estimated from the contours. Data was regenerated for each survey line in this fashion, where only line 2 had sparse contours making it difficult to reconstruct.

Inversion Methodology

The Earth Resources Laboratory has developed modeling and inversion codes which are fast, accurate and stable (Zhang, et. al, 1995; Zhang, et. al., 1996; Shi, 1998). They use finite differences and the bi-conjugate gradient method for both the forward and inverse algorithms. The fundamental equation is Ohm's law, for our interest given by

$$\nabla(\sigma(\mathbf{x})\nabla V(\mathbf{x})) = -I(\mathbf{x}) \qquad (1)$$

where $\mathbf{x}$ is the position vector, σ is conductivity, V is voltage, and I is current. Stability and improved accuracy is achieved in the inversion algorithm by the use of Tikhonov regularization. The objective function $\Psi(m)$, which is minimized is:

$$\Psi(\mathbf{m}) = \|\mathbf{d} - \mathbf{G}(\mathbf{m})\|^2 + \tau\|\mathbf{L}\mathbf{m}\|^2 \qquad (2)$$

where $\mathbf{d}$ = data, $\mathbf{G}$ = model, $\mathbf{L}$ = Laplacian, τ = regularization parameter, and $\mathbf{m}$ = model parameter.

Inversion Results

Individual Lines

Figures 9 to 11 show all the surveys line tomograms plotted on a global log scale ranging from 0 to 3.5, which linearly is equivalent to 1 to 3200 ohm-m. The individual lines show conductive material throughout the region with a few areas of resistive material at Belfond, at depth beneath Sulphur Springs, east of Terre Blanche, and around Belle Plaine.

Line 1 (Figure 9.a) runs west to east and is nearly parallel with the major northernmost caldera fault north of Soufriere. The western end of the line is less than 100 m from Soufriere Bay and the eastern end is northeast of Cresslands. The image shows a large area of less than 10 ohm-m resistivity. The first 500 m of the line from the surface to 800 m depth is in this zone, which narrows to a lens from the surface to 400 m depth to the east and ends at a distance of 2 km. There is a very conductive zone of approximately 3 ohm-m, which runs from a distance of 500 m to 2 km and at a depth from 50 m to 300 m which lies on top of 50 ohm-m to 100 ohm-m material. We may have imaged seawater intrusion from Soufriere Bay and/or fluids related to the major fault.

Line 2 (Figure 9.b) runs parallel to Line 1 about 400 m to the south. Its western edge is right at Soufriere Bay in the middle of Soufriere. The area under the town has resistivities ranging from 30 ohm-m to 100 ohm-m for the top 200 m in depth and then

similar to Line 1 has a large 10 ohm-m and less zone extending to the east which comes to the surface just outside the town for a distance of 1 km. The eastern edge, the last 500 m, becomes more resistive 30 ohm-m to 100 ohm-m.

Line 3 (Figure 9.c) runs towards the northeast starting north of Malgretoute, near Stonefield, and approximately 200 meters from the sea. It has a distinct vertical conductive feature from 1.4 to 2 km distance, which is near two fault junctions. The top of the feature extends out east and west for about 700 meters at depths of 100 to 200 meters. The Diamond Spring is located in this region at a distance of 1.5 km. The remainder of the image is relatively resistive from 50 ohm-m to 100 ohm-m. The geohydrology of the Malgretoute area appears to be different to Soufriere (Lines 1 and 2) as conductive material does not appear given the proximity to the sea. The fault fluids are conductive (3 ohm-m to 7 ohm-m) suggesting the geothermal circulation waters to be somewhat saline.

Line 4 (Figure 9.d) is also oriented towards the northeast starting from the east of Gros Piton near Union Vale and ending near Beausejour. The line is nearly parallel to the major southern caldera fault. The western edge of the line is resistive from the Piton and the middle is conductive with two pockets of conductive material further to the east. The major central conductive feature is from Victoria Junction to the Belle Plaine/Montet Road junction. Etangs located at a position of 2.4 km is one of the recommended drilling sites (Aquater, 1982; LANL, 1984; GENZL, 1992) but yet to be drilled. Several faults intersect this line from 2.5 km in distance to the end of the line.

Line 5 (Figure 10.a) runs north to south, west of the Rabot Ridge. It has no major features with most of the line at 20 to 40 ohm-m.

Line 6 (Figure 10.b) also is north to south to the west of the Rabot Ridge starting just north of the Caldera, near Ruby. The line has a distinct vertical feature at 1.4 km distance, which is close to the Diamond Spring. North of the feature is conductive and to the south is relatively resistive except for a lens at 200 m depth. A NE trending fault intersects the line at approximately 1.5 km in distance.

Line 7 (Figure 10.c) runs north to south, from Ruby through Sulphur Springs and ends at Fond Doux. The image shows the existence of a very resistive layer (over 1000 ohm-m) from beneath Sulphur Springs and extending for 1.5 km at depths greater than 450 m. There is a larger high resistivity zone of over 300 ohm-m, which extends from just north of Sulphur Springs south for 2.2 km. The resististive zone is overlain by a conductive zone of 10 ohm-m and less which comes up to the surface in the area of Sulphur Springs and extends north to the end of the line near Ruby. The Diamond Spring is located at 1 km distance and is clearly connected to the Sulphur Springs. The conductive zone once north of the resistive body covers depths from the surface to nearly 800 m. Also, note the resistive feature from 3.2 km to 4.5 km in distance at the surface that corresponds to the Belfond area.

Line 8 (Figure 10.d) runs on the east of Terre Blanche and appears different to the rest of the lines. It has high resistivities at the surface to a depth of 100 m from distances of 800 m to the end of the line and is also resistive for the first 600 m of the line from 200 m below ground surface (bgs) to depth. The line has two small conductive features of 5 to 10 ohm-m centered at distances of 1.2 km and 2.1 km at a depth of 300 m, which correspond to two faults.

Line 9 (Figure 11.a) runs to the southeast starting from Coubaril passing through Sulphur Springs and ending in Belle Plaine. Line 9 confirms the resistive body beneath Sulphur Springs seen in Line 7 with a resistivity of 300 to 600 ohm-m. Similar to Line 7 it is overlain by a conductive layer of 10 ohm-m and less which extends to the surface at Sulphur Springs. Belfond is highly resistive at the surface to 200 m bgs and is underlain by a conductive pocket. Both ends of the line near the surface are conductive.

Line 10 (Figure 11.b) runs from Belle Plaine southwest to Victoria Junction and is on or near a fault its entire length. Line 10 has a resistive surface of 100 to 200 ohm-m generally underlain by more conductive material. There is a conductive lens (~ 5 ohm-m) from 400 to 1500 m distance at a depth of 200 to 400 m and a pocket centered at 2 km distance and depth of 300 to 500 m. The rest of the image is 12 to 40 ohm-m.

Line 11 (Figure 11.c) runs north to south from Gros Piton to Delcer and has no major features. The entire image is uniform with a range of low resistivities from 10 ohm-m at the surface gradually increasing to 35 ohm-m at depth.

Line 12 (Figure 11.d) runs north to south from Victoria Junction to Le Riche. Line 12 also has no features with nearly uniform low resistivity 20 to 40 ohm-m.

Line 13 was taken well outside the Caldera 4.5 km to the southeast of Line 12 in Londonderry. Line 13 has a resistive feature at a distance of 2 to 2.5 km and 500 m bgs to depth with resistivity of 100 ohm-m. It has a distinct conductive lens of 10 ohm-m and less at depths of 100 to 300 m, which comes to the surface at both ends of the line.

Summary of Lines

At depth, 400 m and greater, there is a resistive zone underneath Sulphur Springs and is overlain by a conductive lens which comes to the surface at the Springs. Also there are two major conductive areas in the caldera. The first is in the north around Diamond, Le Perle, Cresslands and ENE of Soufriere, which comes to the surface in certain locations. It appears to be connected to the conductive zone beneath Sulphur Springs (Figure 10.c). The second is on the southern rim of the caldera from south of Beausejour through Etangs to Union Vale and further south. These two conductive zones run along two faults trending northeast and are connected north to south along the fault running through Sulphur Springs.

Accuracy

The survey lines have thirteen locations where two or more lines intersect affording us a check of accuracy by comparing the resistivity values from different lines at these same locations. Figure 12 shows eight vertical slices at cross-locations from throughout the caldera. The checks are generally good with 7 of the 13 crosses showing very good correlations similar to Figure 12(a,b,c,d,h). The remainder 6 show the same trends in resistivity however offset vertically in depth such as in Figure 12(e,f,g). There are no major errors on the order of magnitude differences in resistivity.

A gauge of the validity of our data reconstruction was obtained by comparing tomograms of Line 9 from the actual apparent resistivity data and that generated from the contour plot of the same data. The images in general have great similarity but as expected the tomogram from reconstructed data lacks some of the detail of the actual data and has a different resistivity scale (Figure 13). The reconstructed tomogram has completed missed the continuation of the circulation fluids at depth to the north of Sulphur Springs and the connectivity of the conductive zone beneath Belfond to Sulphur Springs. Also, the maximum resistivity is 794 ohm-m compared to 19,950 ohm-m for the actual data tomogram and the minimum resistivity values are equivalent at 1.21 and 1.27 ohm-m. The major features are similar in both images showing a resistive body at depth beneath Sulphur Springs overlain by a conductive layer which comes to the surface at Sulphur Springs, a resistive block at the surface at Belfond, a relatively resistive block 1000 meters to the north of the emanations, and conductive material beneath Belfond. Also of note is the difference in shape of the resistive body at depth. The features observed in the

tomograms of the other lines are valid in depth and location based upon the comparison from Line 9.

3D Interpolation

Knowing the locations of the lines the 2D data was interpolated to generate a 3D rendered resistivity structure for the Qualibou Caldera. A note of *caution* the 3D rendering is an interpolation of already imperfect 2D data. Also the 3D rendering assumes the same surface elevation for all the data, not accounting for topography. It is *not* equivalent to acquiring and inverting 3D data. Rendering in 3D is the best, which could be done with the present available data.

Depth Slices

Figures 14 and 15 show two depth slices at 200 m and 700 m bgs to highlight the conductive zone and the resistive body beneath Sulphur Springs. The shallow image at 200 m bgs shows several relative resisitive (30 to 100 ohm-m) areas; Stonefield to Petit Piton, Belle Plaine - Beausejour, Belfond, east of La Perle, and the southeast edge. The remainder of the area is conductive (15 ohm-m and less) with a very conductive zone just northeast of Soufriere along the caldera fault. Two sharp resistivity contrasts exist just south of Beausejour and the boundary of the Rabot ridge to Jalousie.

The deeper 700 m bgs image is highlighted by the major resistive body centered around Sulphur Springs approximately 4 square kilometers in area. The resistive zone is clearly

bounded by faults delineating the extent of the heat source of Sulphur Springs. The Diamond Spring is just north of the northern fault and therefore on the edge of the heat source. There are two conductive features running west to east at distances of 3 and 7 km north, where the southern zone runs through Etangs and the northern one through La Perle.

Vertical Slices

Figures 16 shows two vertical slices directly north-south and west-east through Sulphur Springs. The north-south slice (Figure 16.a) shows the Sulphur Springs resistive body and clearly highlights fluid circulation around the heat source due to convection. The west-east slice (Figure 16.b) also shows a similar system, however it is sharply bounded on the west by a curvilinear fault (Rabot Ridge).

Volumetric Surfaces

Volumetric surfaces of equal and lower or higher resistivity where generated from the 3D rendered data. The results (Figure 17) are fascinating, as they appear to show a classic vapor dominated geothermal system with a resistive body overlain by circulation fluids descending around the margins. Figure 18 shows volumes from a top view (displaying values from all depths projected to the surface) for varying resistivities. Several small conductive, less than 3 ohm-m, pockets appear on the northern caldera fault northeast of Soufriere, at Diamond and Cresslands, around Sulphur Springs, southeast of Sulphur

Springs, and near Fond Doux (Figure 18.a). In comparison, a large area has 10 ohm-m and less material, with a north-northwest trend (Figure18.c). The most resistive, greater than 1000 ohm-m, zone is confined to the area of the Sulphur Springs (Figure 18.f) and the 100 ohm-m and greater area is bounded by the fault structure (Figure 18.d).

Line 9 Comparisons Past and Present

As stated earlier, Greenwood and Lee employed the best available modeling capability of their day to generate a detailed resistivity model of Line 9. Figure 19 shows this 1976 model colorized and the recently reinverted tomogram for Line 9. The two images have similar features, a very conductive surface zone at Sulphur Springs and the resistive block at the surface south of Sulphur Springs. However, the most important feature of the tomogram, a resistive zone at depth, is not seen in the 1976 model. The model does show a slightly more resistive feature in the center and a conductive zone to the south at depth, which is the correct trend, but in error on the order of two magnitudes. Considering the computing interpretation limitations at the time the model was generated it did well for the top 200 m. An analysis of Line 9 specific to the Sulphur Springs was performed (Morgan, et al., Resistivity tomogram of a 4.5 km line through the Sulphur Springs, St. Lucia, submitted to the *The Leading Edge*, 2002) which discusses the Lee and Greenwood (1976) models of line 9 in more detail.

Interpretation

Analysis of existing data (Aquater, 1982; LANL, 1984; GENZL, 1992) has shown that a vapor dominated geothermal system is present. Clearly the results have confirmed this model with the existence of a resistive body under Sulphur Springs. At depths up to 300 meters fluids are well connected throughout the region. The dominant flow direction is south-north, possibly being fed from the south and discharging to the north (Figure 10.c). The two main caldera faults appear to be flow channels as resistivities are conductive at all depths along the fault locations. The northern NE trending faults could be acting as barriers to northward flow providing a source to the La Perle, Diamond, Cresslands areas. The results show briny fluids coming to the surface at Sulphur Springs and in the Diamond - La Perle area where there are known hot springs. Hydrogeochemical analysis points to the same source reservoir for Sulphur Springs and the outlying thermal springs. The connectivity of the conductive zone supports this conclusion and also shows connectivity to the southeast of Sulphur Springs as well, an interesting area for geothermal exploration. The structure system of the caldera is the dominant controlling feature; bounding the heat source and providing permeability for fluid movement.

Non-Uniqueness

The conductive features that we have interpreted as thermal convective plumes of the geothermal system could have low resistivities due to several factors therefore the interpretation has non-uniqueness. The resistivity of a rock is inversely proportional to roughly the square of its porosity from Archie's Law and directly proportional to the solution resistivity (Telford, et al., 1990). Therefore, the conductive features observed in

our results may be areas of relatively high porosity or zones of lower solution resistivity. Another factor to consider is the effect of temperature on resistivity, where a rise of 1^0C lowers solution resistivity by 2%. Considering the Sulphur Springs region could have temperature variations of over 200^0C (Williamson, 1979) that would lower solution resistivity by at least 400% or a factor of 4. The conductive features could be due to variable lithology (high porosity areas) or zones of hot gases such as at Sulphur Springs, where a conductive zone comes to the surface.

Conclusions

The novel concept of reconstructing and inverting old pseudo section data contours is proven not only to be feasible but greatly enhancing to the interpretation of the data. Two questions remain in regard to the observed conductive features; are they truly a brine or a result of non-uniqueness and are they hot or cold? Five main conclusions can be stated based on the MIT reinterpretation:

(1) The question of a resistive body beneath Sulphur Springs has been definitively answered in the affirmative. The high resistivity values of over 1000 ohm-m at depth correspond with the hypothesized vapor dominated system at Sulphur Springs.

(2) The 3D rendered images have delineated conductive zones that may be circulation fluids showing descending waters on the margins of the geothermal system.

(3) The extent of the heat source has been defined beneath Sulphur Springs.

(4) Possible fluid connectivity between the Sulphur Springs and Diamond shown.

(5) Based on the results, recommended drilling locations are Diamond, Etangs, and just southeast of Sulphur Springs. These areas may have different chemistry to the Sulphur Springs making geothermal production feasible.

References

Aquater S.p.A, Exploration of St. Lucia's geothermal resources, *Government St. Lucia*, Ministry of Finance and Planning, 1982.

Bath, A.H., Summary of chemical data from Sulphur Springs thermal area, St. Lucia, West Indies, WD/OS/76/21, *Institute of Geological Sciences*, Oxfordshire, England, 1976.

Gandino, A., Piovesana, F., Rossi, R., and Zan, L., Preliminary evaluation of Soufriere Geothermal field, St. Lucia (Lesser Antilles), *Geothermics*, 14, 577-590, 1985.

Geothermal Energy New Zealand Limited (GENZL), St. Lucia Geothermal Project, St. Lucia Electricity Services Limited, 1992.

Goff, F., and Vuataz, F., Hydrogeochemistry of the Qualibou Caldera geothermal system, St. Lucia, West Indies, *Transactions Geothermal Research Council*, 8, 377-382, 1984.

Greenwood, P.G., and Lee, M.K., Geophysical surveys in St. Lucia for geothermal resources, *Institute of Geological Sciences*, Geophysical Division, London, 1976.

Kruger, P. and Otte, C., Geothermal energy: resources, production, stimulation. *Stanford University Press*, 1973.

Lee, M.K., and Greenwood, P.G., The interpretation of resistivity surveys for geothermal resources in St. Lucia*, Institute of Geological Sciences*, Applied Geophysics Unit, Report No. 31, London, 1976.

Los Alamos National Laboratory (LANL), Evaluation of the Saint Lucia geothermal Resource: geologic, geophysical, and hydrogeochemical investigations, LA-10234-MS, 1984.

Merz and McLellan, Report on exploration and drilling at Soufriere, *Ministry of Overseas Development*, London and Government of St. Lucia, 1977.

Shi, W., Advanced modeling and inversion techniques for three dimensional geoelectrical surveys, Ph.D. Thesis, *Massachusetts Institute of Technology*, 1998.

Telford, W.M., Geldart, L.P., and Sheriff, R.E., 1990. *Applied Geophysics*, 2nd Edition. Cambridge Univeristy Press.

White, D.E., Muffler, L.J.P., and Truesdell, A.H., Vapor-dominated hydrothermal systems compared with hot-water systems, *Economic Geology*, 66, 75-97, 1971.

Williamson, K.H., A model for the Sulphur Springs geothermal field, St. Lucia, *Geothermics*, 8, 75-83, 1979.

Wohletz, K., Heiken, G., Ander, M., Goff, F., Vuataz, F.D., and Wadge, G., The Qualibou Caldera, St. Lucia, West Indies, *Journal of Volcanology and Geothermal Research*, 27, 77-115, 1986.

Zhang, J., Mackie, R.L., and Madden, T.R., Three-dimensional resistivity forward modeling and inversion using conjugate gradients, *Geophysics*, 60, 1313-1325, 1995.

Zhang, J., Rodi, W., Mackie, R.L., and Shi, W., Regularization in 3-D dc resistivity tomography, SAGEEP, *Environmental and Engineering Geophysical Society*, 130-135, 1996.

Figure Captions

Figure 1: Location of Saint Lucia, West Indies

Figure 2: Geology map of Qualibou Caldera (from Greenwood and Lee, 1976)

Figure 3: Structure of the Qualibou Caldera, compiled from Aquater S.p.A (1982), Gandino et al. (1985), Los Alamos National Laboratory (1984).

Figure 4: Map of survey lines (from Greenwood and Lee, 1976)

Figure 5: Map of study area

Figure 6: Example of dipole-dipole contour plots of apparent resistivity data (from Greenwoods and Lee, 1976)

Figure 7: Line 9 best interpretation model (from Lee and Greenwood, 1976)

Figure 8: Example of pseudo-section reconstruction

Figure 9: Tomograms a) Line 1, b) Line 2, c) Line 3, d) Line 4

Figure 10: Tomograms a) Line 5, b) Line 6, c) Line 7, d) Line 8

Figure 11: Tomograms a) Line 9, b) Line 10, c) Line 11, d) Line 12

Figure 12: Check of resistivity accuracy at survey line intersections. Values are log resistivity (ohm-m).

Figure 13: Line 9 Tomograms log resistivity (ohm-m)

Figure 14: Log resistivity (ohm-m) slice at 200 m bgs

Figure 15: Log resistivity (ohm-m) slice at 700 m bgs

Figure 16: Vertical log resistivity (ohm-m) slices through Sulphur Springs

Figure 17: Volumetric resistivity images

Figure 18: Volumetric resistivity images from top (surface) view

Figure 19: Line 9 interpretation past and present: a) Lee and Greenwood (1976) Model, b) MIT 2000 Tomogram

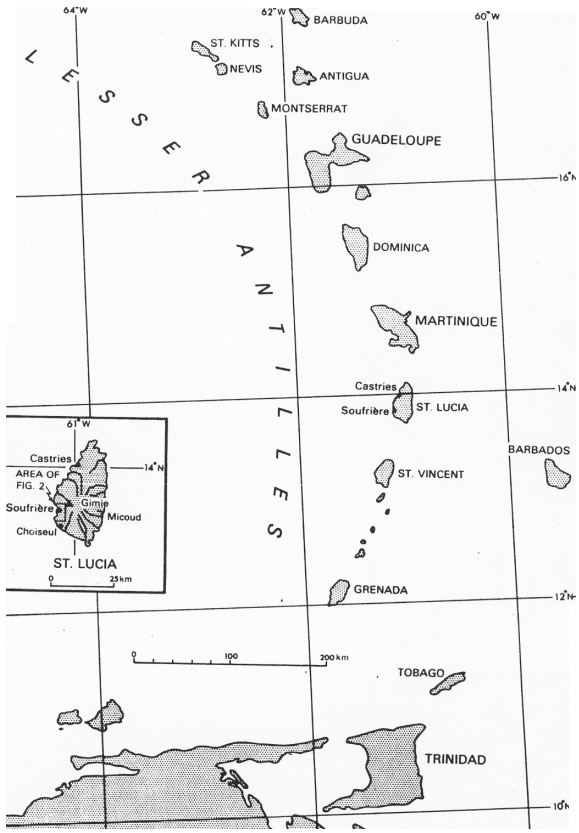

Figure 1: Location of Saint Lucia, West Indies

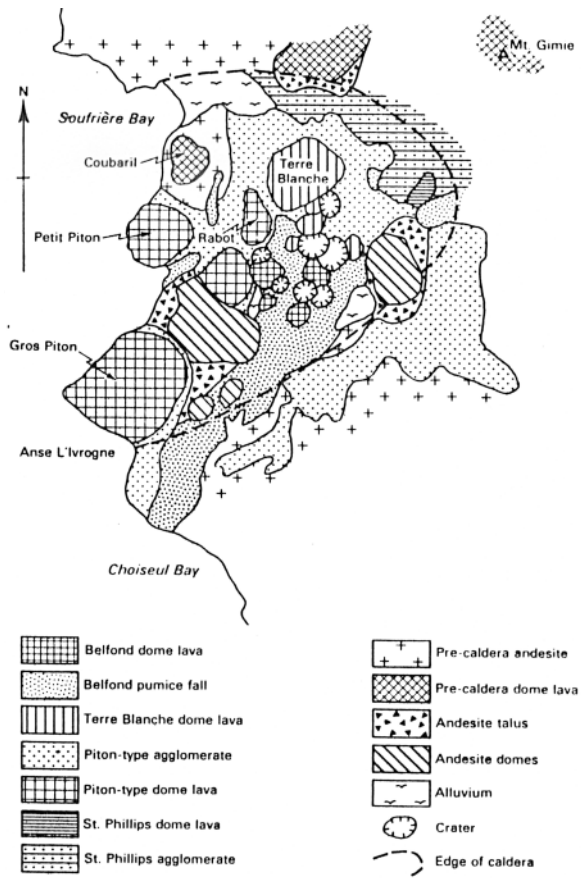

Figure 2: Geology map of Qualibou Caldera (from Greenwood and Lee, 1976)

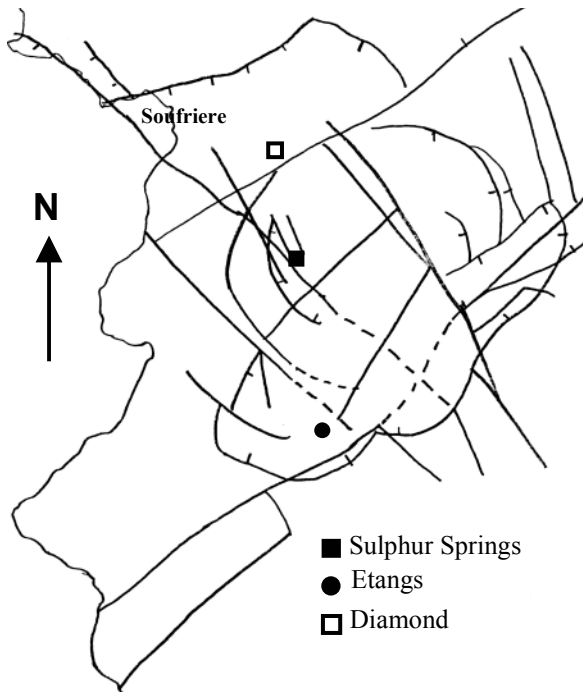

Figure 3: Structure of the Qualibou Caldera, compiled from Aquater S.p.A (1982), Gandino et al. (1985), Los Alamos National Laboratory (1984).

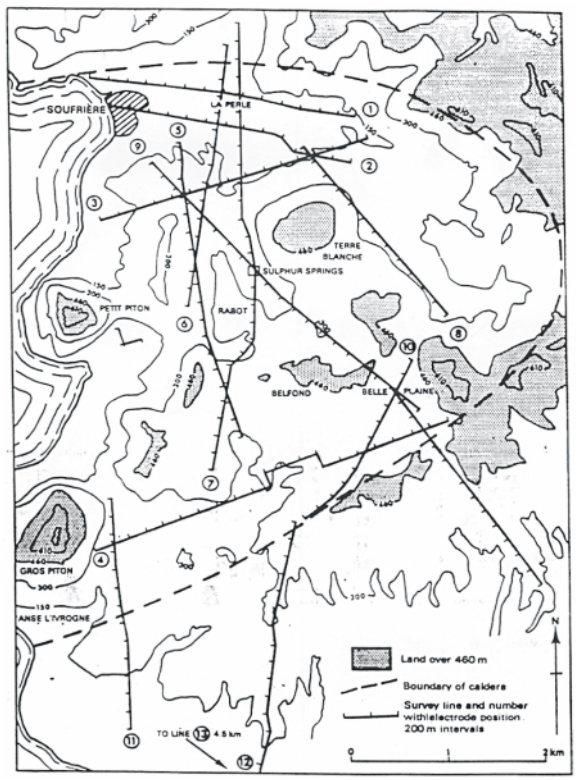

Figure 4: Map of survey lines (from Greenwood and Lee, 1976)

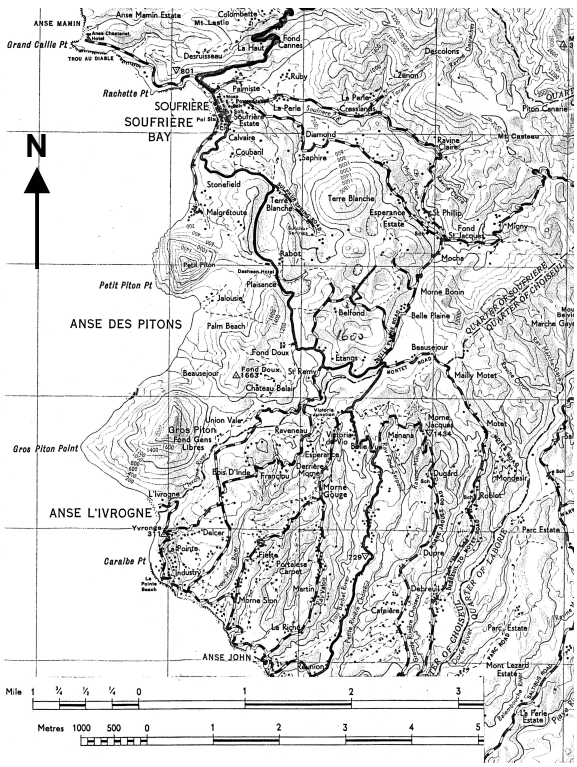

Figure 5: Map of study area

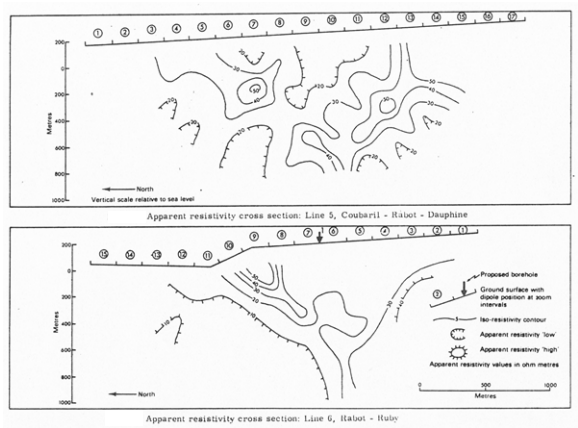

Figure 6: Example of dipole-dipole contour plots of apparent resistivity data (from Greenwood and Lee, 1976)

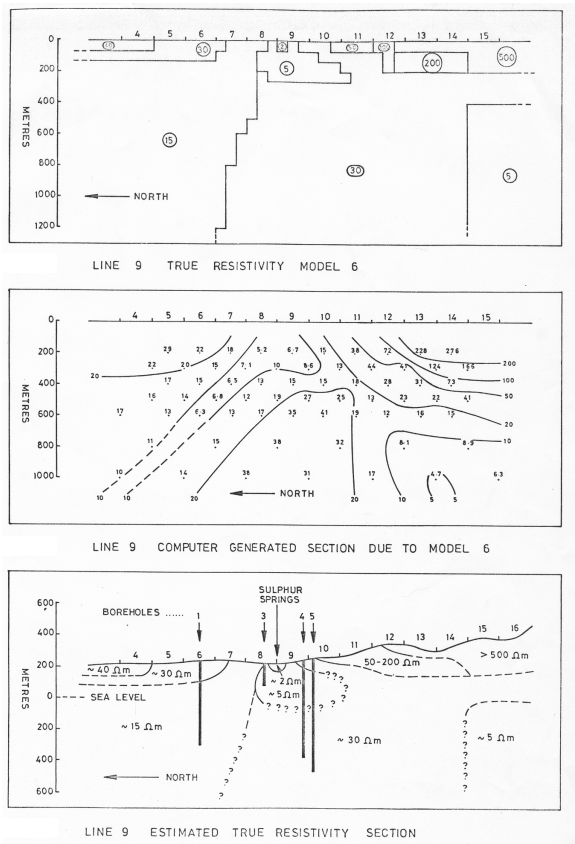

Figure 7: Line 9 best interpretation model (from Lee and Greenwood, 1976)

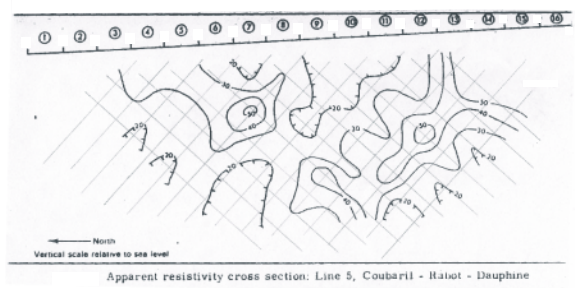

Figure 8: Example of pseudo-section reconstruction

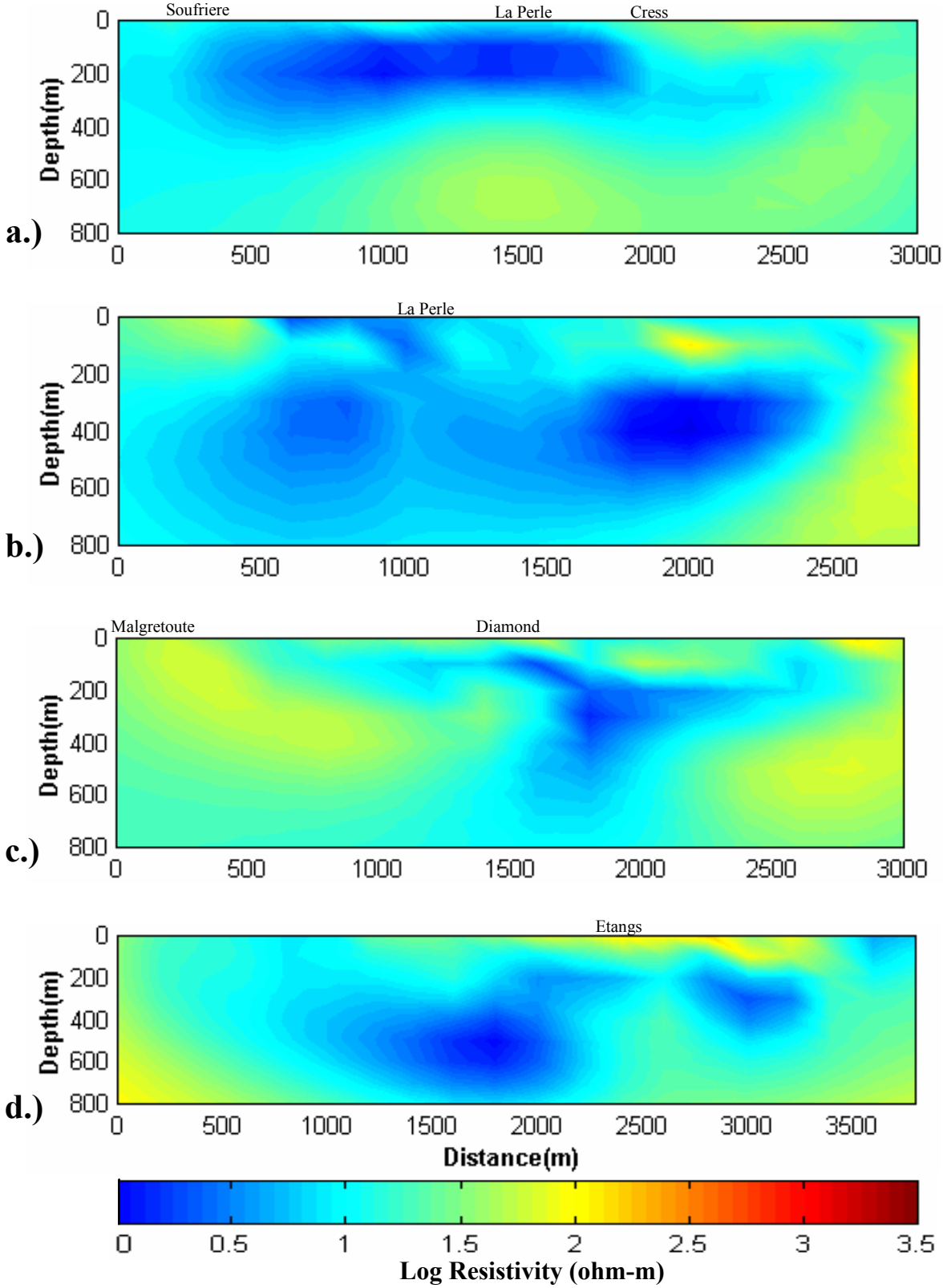

Figure 9: Tomograms a) Line 1, b) Line 2, c) Line 3, d) Line 4

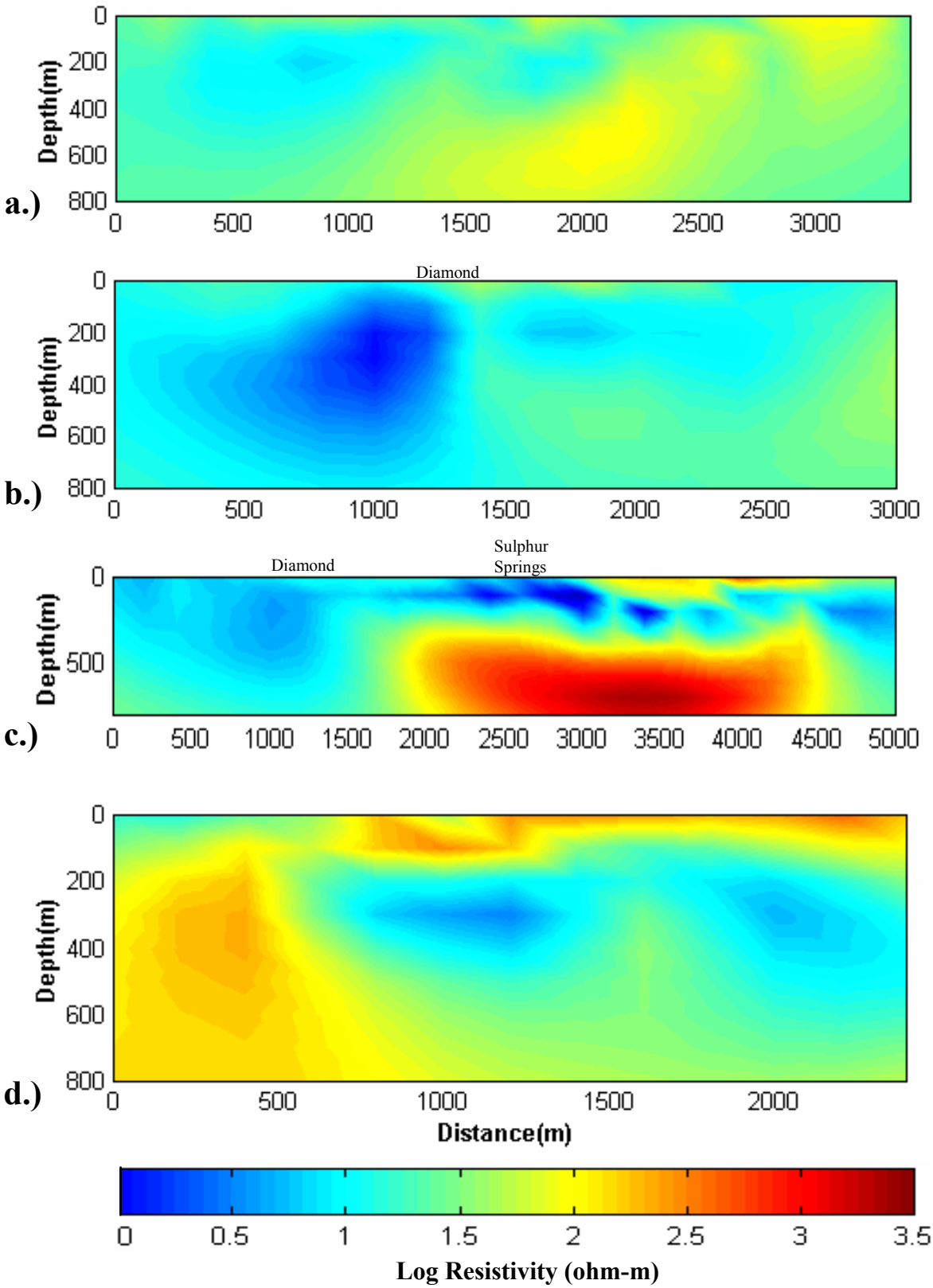

Figure 10: Tomograms a) Line 5, b) Line 6, c) Line 7, d) Line 8

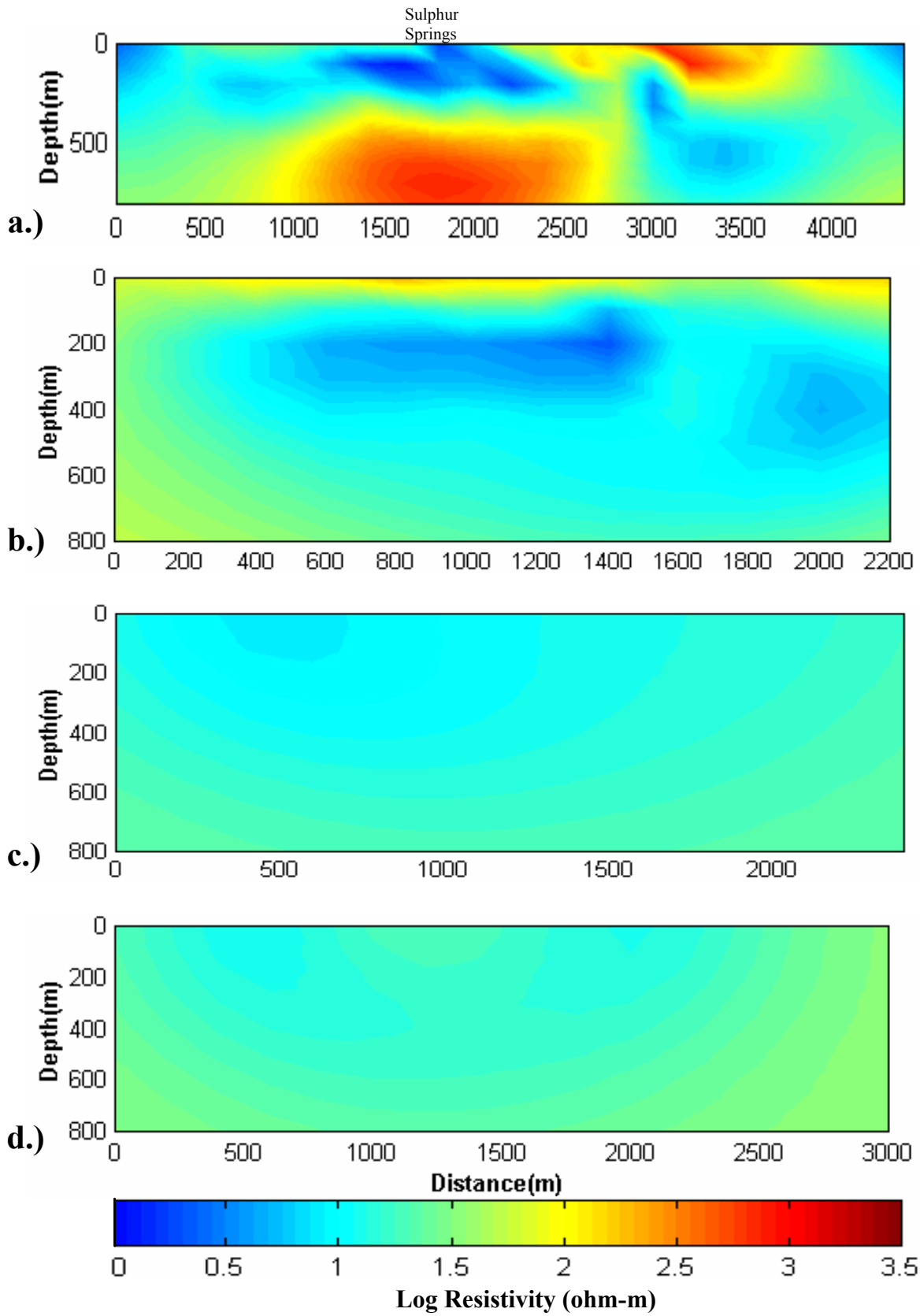

Figure 11: Tomograms a) Line 9, b) Line 10, c) Line 11, d) Line 12

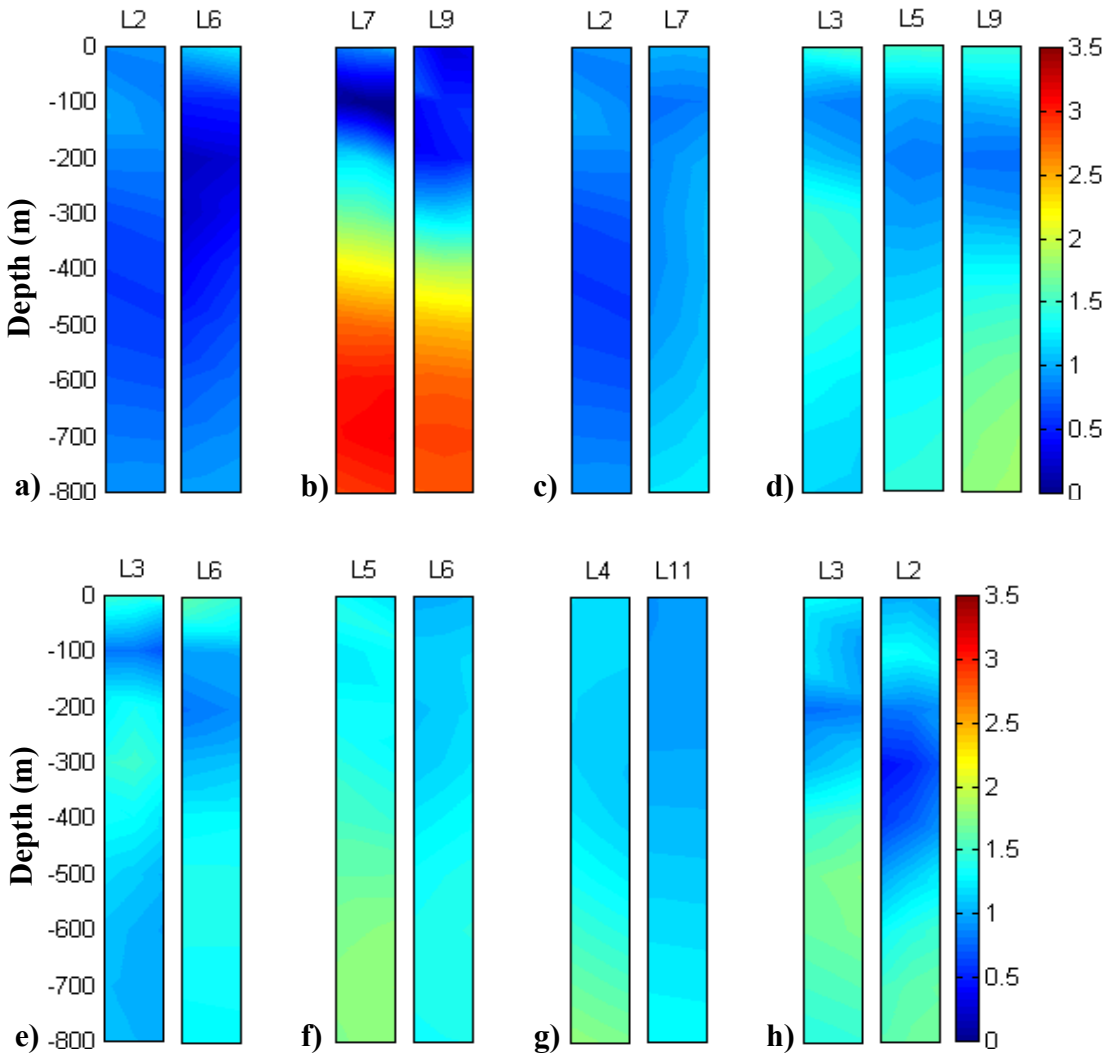

Figure 12: Check of resistivity accuracy at survey line intersections. Values are log resistivity (ohm-m)

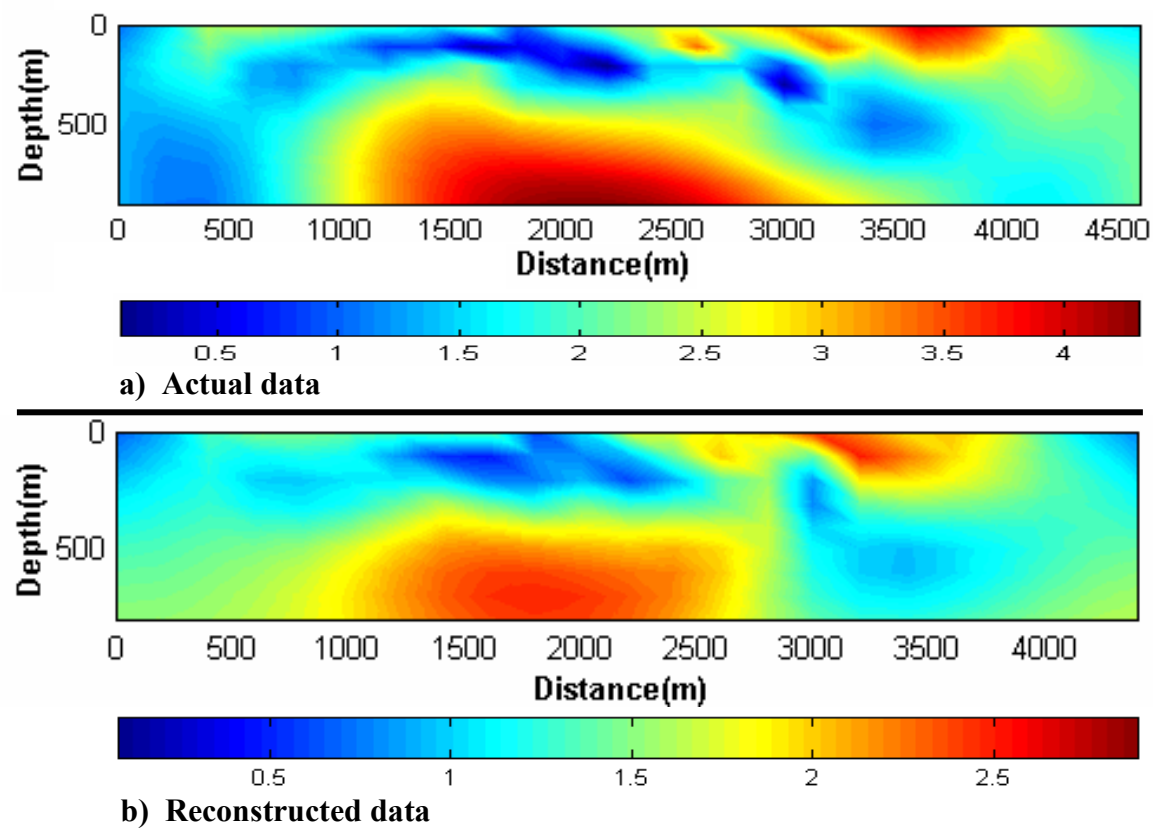

Figure 13: Line 9 tomograms log resistivity (ohm-m)

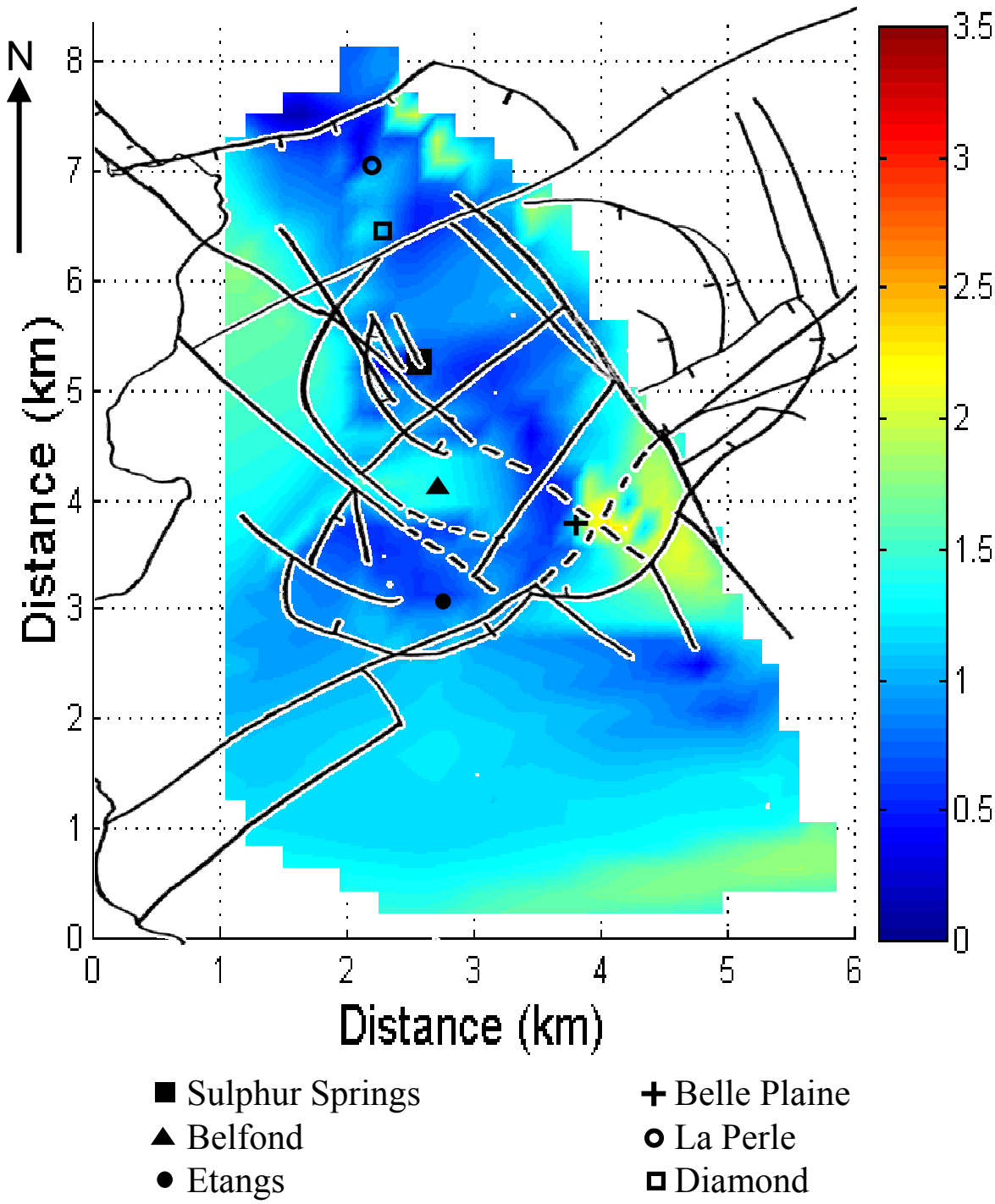

Figure 14: Log resistivity (ohm-m) slice at 200 m bgs

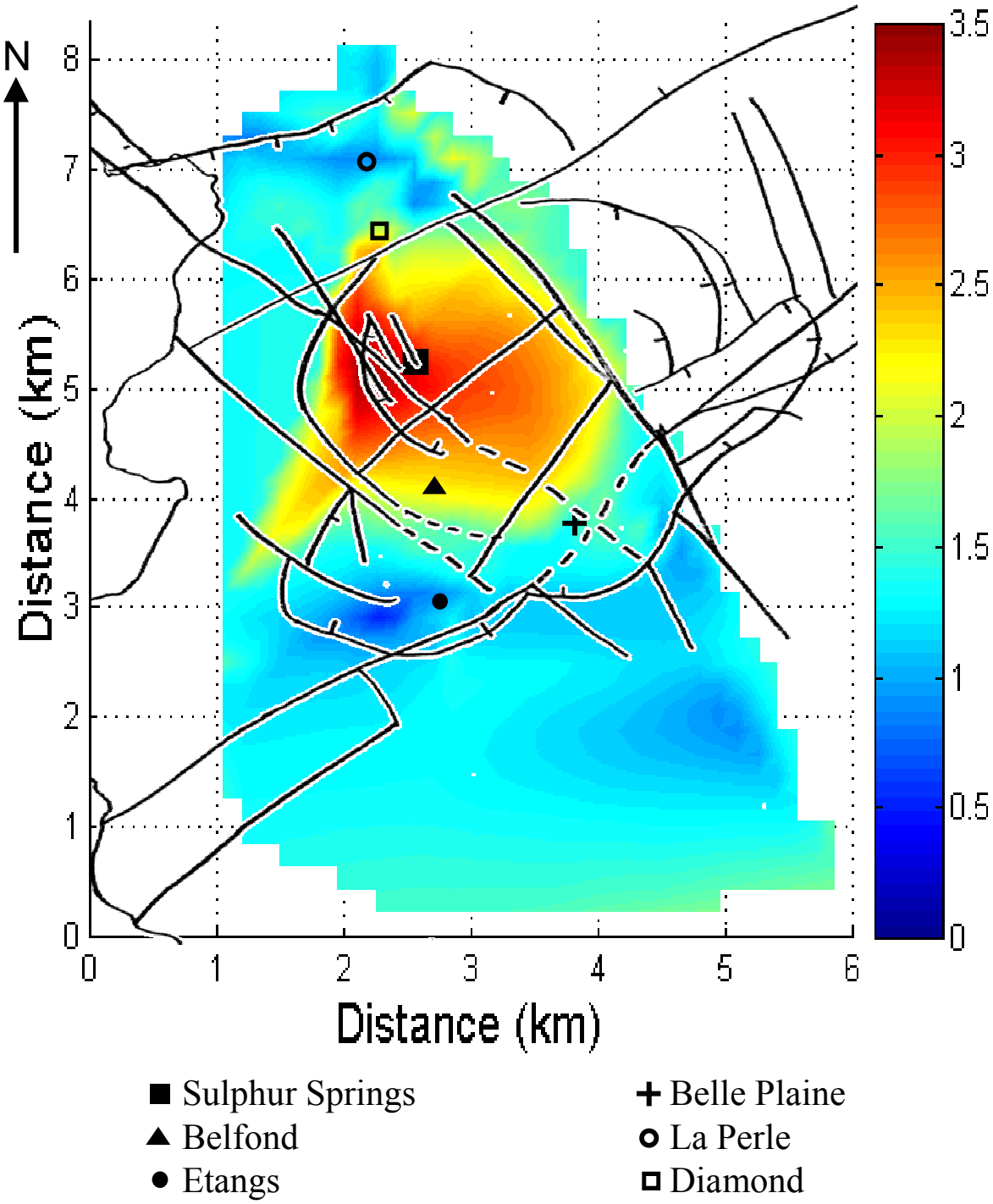

Figure 15: Log resistivity (ohm-m) slice at 700 m bgs

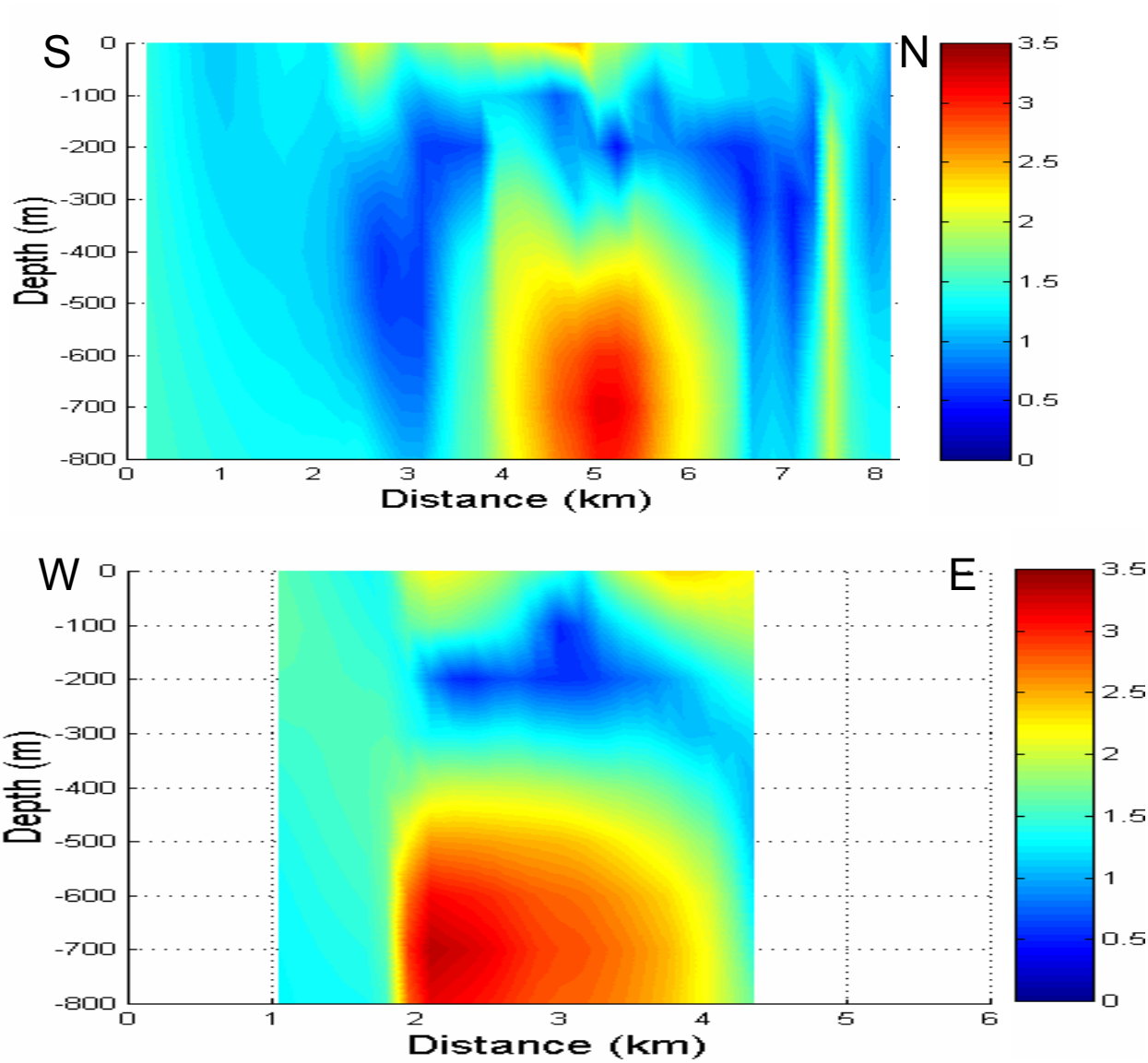

Figure 16: Vertical log resistivity (ohm-m) slices through Sulphur Springs

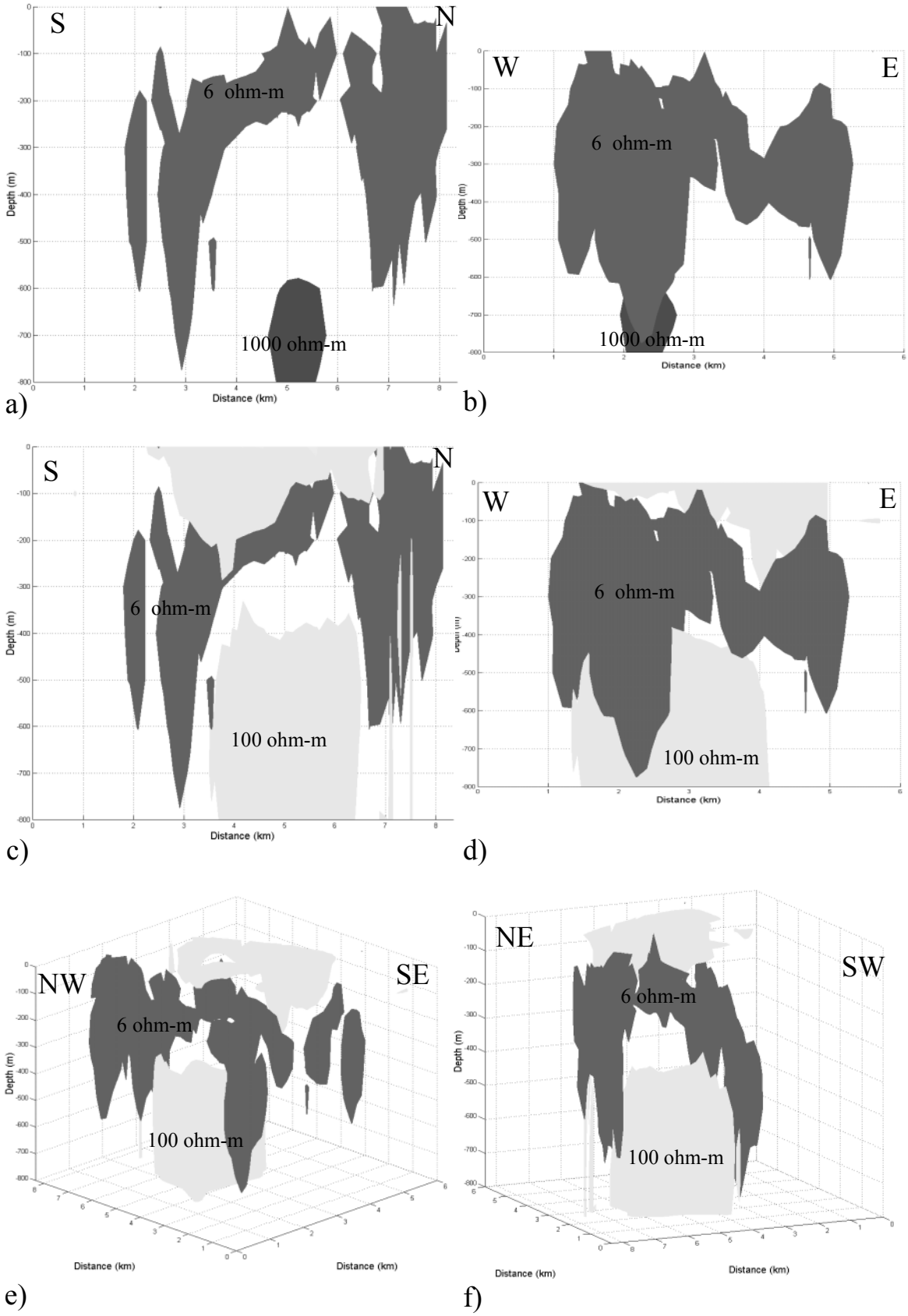

Figure 17: Volumetric resistivity images

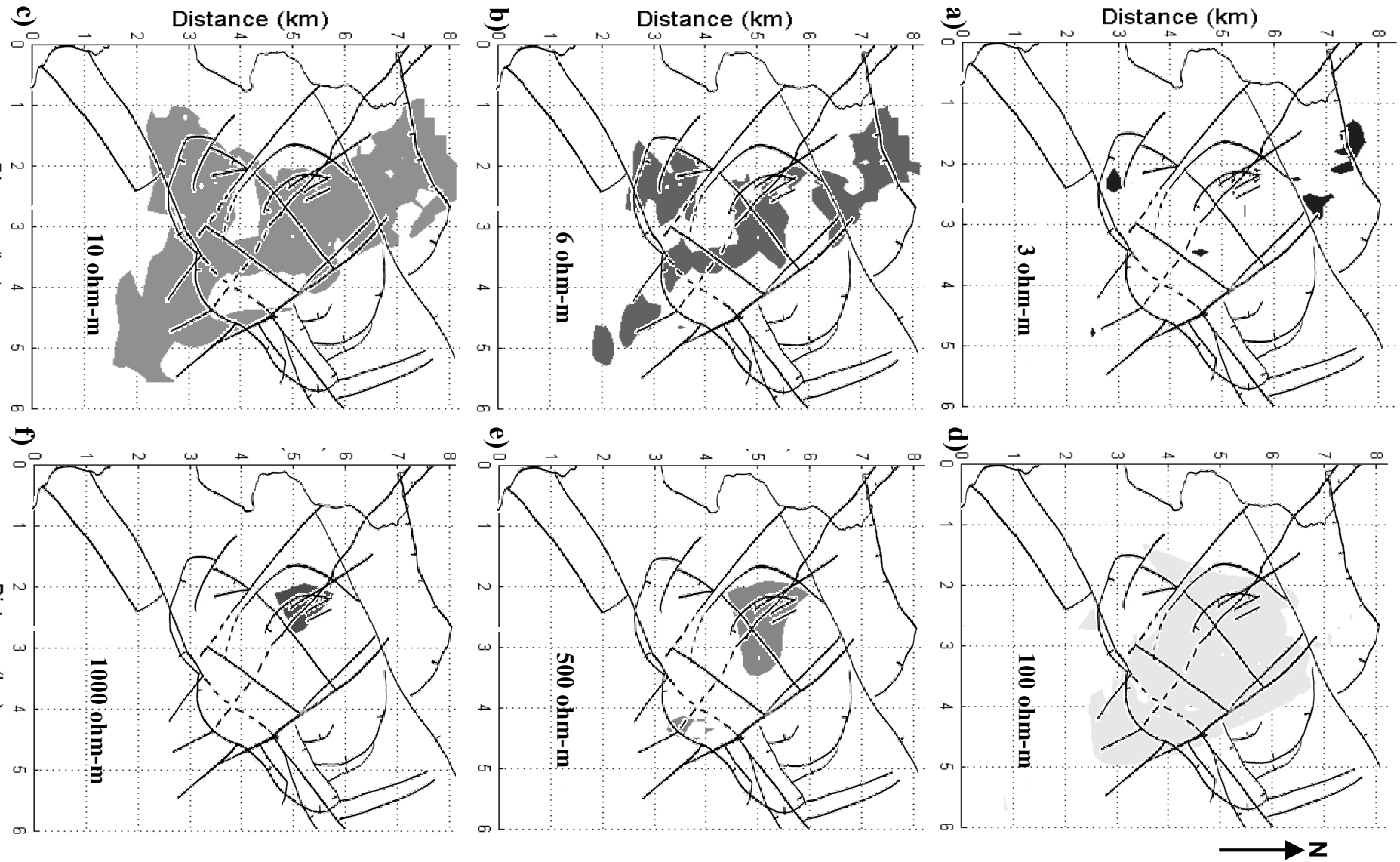

Figure 18: Volumetric resistivity images from top (surface) view

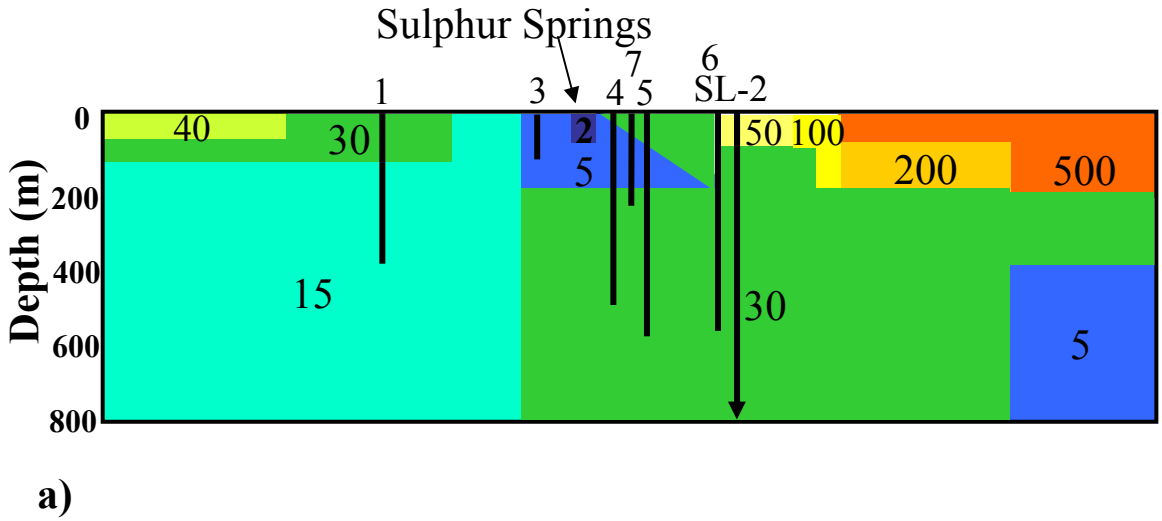

a)

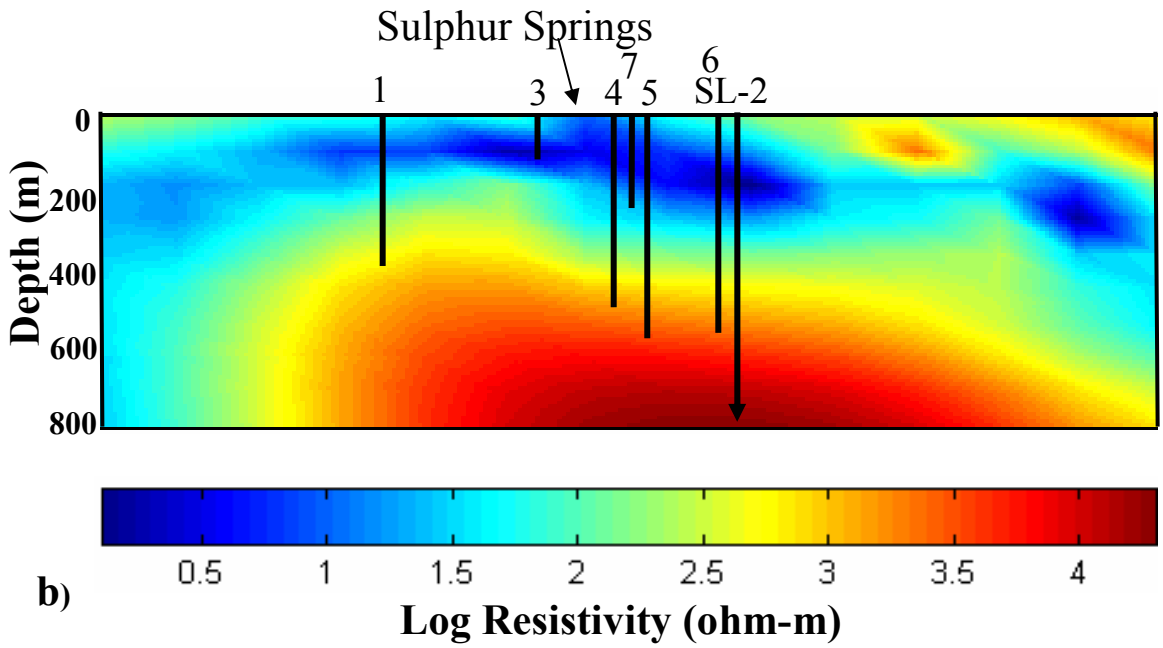

b)

Figure 19: Line 9 interpretation past and present:
a) Lee and Greenwood (1976) Model, b) MIT 2000 Tomogram